AGU PUBLICATIONS

JGR

Journal of Geophysical Research: Space Physics

RESEARCH ARTICLE

10.1002/2017JA023919

Key Points:
- Long-term analysis of the horizontal parameter of wave structures observed by airglow imager
- Clear seasonal variation of propagation direction of gravity waves in mesopause region
- Relationship between medium-scale traveling ionospheric disturbances and solar activity

Correspondence to:
K. Shiokawa,
shiokawa@nagoya-u.jp

Citation:
Takeo, D., K. Shiokawa, H. Fujinami, Y. Otsuka, T. S. Matsuda, M. K. Ejiri, T. Nakamura, and M. Yamamoto (2017), Sixteen year variation of horizontal phase velocity and propagation direction of mesospheric and thermospheric waves in airglow images at Shigaraki, Japan, *J. Geophys. Res. Space Physics*, *122*, doi:10.1002/2017JA023919.

Received 18 JAN 2017
Accepted 17 JUL 2017
Accepted article online 20 JUL 2017

Sixteen year variation of horizontal phase velocity and propagation direction of mesospheric and thermospheric waves in airglow images at Shigaraki, Japan

D. Takeo[1], K. Shiokawa[1], H. Fujinami[1], Y. Otsuka[1], T. S. Matsuda[2], M. K. Ejiri[2], T. Nakamura[2], and M. Yamamoto[3]

[1]Institute for Space-Earth Environmental Research, Nagoya University, Nagoya, Japan, [2]National Institute of Polar Research, Tachikawa, Japan, [3]Research Institute for Sustainable Humanosphere, Kyoto University, Uji, Japan

Abstract We analyzed the horizontal phase velocity of gravity waves and medium-scale traveling ionospheric disturbances (MSTIDs) by using the three-dimensional fast Fourier transform method developed by Matsuda et al. (2014) for 557.7 nm (altitude: 90–100 km) and 630.0 nm (altitude: 200–300 km) airglow images obtained at Shigaraki MU Observatory (34.8°N, 136.1°E, dip angle: 49°) over ~16 years from 16 March 1999 to 20 February 2015. The analysis of 557.7 nm airglow images shows clear seasonal variation of the propagation direction of gravity waves in the mesopause region. In spring, summer, fall, and winter, the peak directions are northeastward, northeastward, northwestward, and southwestward, respectively. The difference in east-west propagation direction between summer and winter is probably caused by the wind filtering effect due to the zonal mesospheric jet. Comparison with tropospheric reanalysis data shows that the difference in north-south propagation direction between summer and winter is caused by differences in the latitudinal location of wave sources due to convective activity in the troposphere relative to Shigaraki. The analysis of 630.0 nm airglow images shows that the propagation direction of MSTIDs is mainly southwestward with a minor northeastward component throughout the 16 years. A clear negative correlation is seen between the yearly power spectral density of MSTIDs and $F_{10.7}$ solar flux. This negative correlation with solar activity may be explained by the linear growth rate of the Perkins instability and secondary wave generation of gravity waves in the thermosphere.

1. Introduction

Many studies have investigated wave-like structures in the upper atmosphere, such as gravity waves and medium-scale traveling ionospheric disturbances (MSTIDs) by using measurement techniques such as radar, lidar, and optical airglow imaging. Radar and lidar observations provide the vertical structure of these waves with high spatial resolution. However, it is difficult to observe the horizontal structure of gravity waves by using these measurement techniques. In contrast, airglow imaging is useful for investigating the two-dimensional horizontal structure of waves in the upper atmosphere, providing the horizontal phase velocity with high spatial and temporal resolutions. There are two major airglow line emissions from the atomic oxygen at wavelengths of 557.7 nm at altitudes of 90–100 km and 630.0 nm at altitudes of 200–300 km. The former emission can be used as a manifestation of atmospheric density variations in the mesopause region, while the latter emission represents variations of both atmospheric and plasma density variations in the bottomside of the ionospheric *F* layer.

Gravity waves affect the wind field and thermal balance in the mesosphere and lower thermosphere region and cause large-scale pole-to-pole circulation, because the waves propagate from the lower to the upper atmosphere with momentum transport. The vertical propagation of gravity waves and its momentum transport depend on the horizontal phase velocity of gravity waves according to the dispersion relation of waves. Therefore, the study of the horizontal phase velocity of gravity waves is important.

The horizontal parameters of waves have been examined in many studies by using airglow images [e.g., *Taylor et al*., 1993; *Hecht et al*., 1994; *Swenson et al*., 1999; *Yue et al*., 2010]. *Nakamura et al.* [1999] made 18 month long-term imaging observations of gravity waves at Shigaraki, Japan, and discussed the seasonal variation of the

propagation direction of gravity waves. *Ejiri et al.* [2003] also investigated the seasonal variation of the propagation direction of gravity waves at Shigaraki and Rikubetsu, Japan, for 1 year. However, long-term variations in small-scale gravity waves observed by airglow imagers for more than 10 years have not been studied yet, because previous studies were performed by visual inspection, which requires a long time to analyze a large number of airglow images. Recently, *Matsuda et al.* [2014] developed a three-dimensional fast Fourier transform (3-D FFT) method to obtain the power spectra of airglow intensity variation in the horizontal phase velocity domain. This method is suitable for rapidly deriving the horizontal phase velocity characteristics of atmospheric gravity waves from a large amount of imaging data.

MSTIDs also have been studied by using airglow images [e.g., *Garcia et al*., 2000; *Makela and Kelley*., 2003; *Martinis et al*., 2010; *Narayanan et al*., 2014]. *Taylor et al.* [1998] reported MSTID observations during the Sporadic *E* Experiment over Kyushu (SEEK) campaign. These were the first 630.0 nm airglow measurements of nighttime MSTIDs in Japan. *Kubota et al.* [2000] and *Saito et al.* [2001] observed sequential MSTIDs, which propagated southwestward over Japan, by using five airglow imager sites in Japan. *Shiokawa et al.* [2003a] performed statistical analysis of MSTIDs obtained at two airglow imager sites in Japan by visual inspection. However, long-term variations of MSTIDs observed by airglow imaging for more than 10 years have not yet been studied.

In this study, we used the 3-D FFT method developed by *Matsuda et al.* [2014] to analyze the horizontal phase velocity spectrum of gravity waves and MSTIDs by using 557.7 nm (altitude of 90–100 km) and 630.0 nm (altitude of 200–300 km) airglow images obtained at Shigaraki MU Observatory (34.8°N, 136.1°E) over ~16 years. This study enables us to investigate the long-term variation of horizontal phase velocity and the propagation direction of gravity waves and MSTIDs and their relationship to other atmospheric and solar activity parameters.

2. Observation

We used airglow images at Shigaraki MU Observatory that were collected over ~16 years from 16 March 1999 to 20 February 2015 by the all-sky airglow imager No. 1 of the Optical Mesosphere Thermosphere Imagers owned by the Institute for Space-Earth Environmental Research, Nagoya University [*Shiokawa et al*., 1999, 2009]. This system has a fish-eye lens with a field of view of 180°, multiple interference filters with a wheel to change filters, and a cooled charge-coupled device (CCD) camera with a resolution of 512 × 512 pixels. The imager 1 was calibrated on 8 January 1998, 12 December 2000, 26 October 2006, 21 February 2007, and 19 April 2012, by using calibration facilities in the National Institute of Polar Research, Japan. The wavelengths of airglow images we used were 557.7 nm in the mesopause region (altitudes from 90 to 100 km) and 630.0 nm in the thermosphere (altitudes from 200 to 300 km). The sampling periods of these airglow images were 5 min (16 March 1999 to 9 July 2000) or 5.5 min (10 July 2000 to 20 February 2015) for each wavelength. We used airglow images only during clear-sky nights because we could not observe gravity waves when there was contamination by clouds.

3. Analysis Method

We used the 3-D FFT method developed by *Matsuda et al.* [2014] to obtain the three-dimensional wave number spectrum of the periodic structures in airglow images. There have been many studies of gravity waves that have analyzed airglow images by visual inspection. However, visual inspection is time consuming and causes artificial bias depending on the person analyzing the images. In contrast, the horizontal phase velocity spectrum can be obtained easily by the 3-D FFT analysis method.

First, we removed dark counts and the offset of the CCD camera by subtracting the average counts at the four corners of the images where the sky image was not projected. We assume that the dark count is uniform over the CCD array. We also removed localized bright spots caused by stars by using an 11 pixel median filter. Next, we calculated the absolute intensity of the airglow at each image pixel by subtracting the contamination of the background continuum emission, which was passed through the 557.7 and 630.0 nm band-pass filters. The intensity of the background continuum emission was measured by a 572.5 nm band-pass filter every 30 min, and we assumed that the intensity was the same at 572.5, 557.7, and 630.0 nm. We calculated the normalized perturbation of the airglow intensity, $\Delta I_i = (I_i - \bar{I})/\bar{I}$, where I_i and $\bar{I}$ are the airglow intensities at the considered time and averaged over ±30 min of the time, respectively. Next, we converted the all-sky images obtained by the fish-eye lens to equidistant coordinates with horizontal sizes of 400×400 km for the 557.7 nm

images and 800 × 800 km for the 630.0 nm images. For this conversion, we assumed airglow heights of 95 km for the 557.7 nm images and 250 km for the 630.0 nm images. *Shefov et al.* [2007] has shown that the height variation of 630 nm emission layer is less than ±20 km during solar maximum and minimum periods. Next, we used the 3-D FFT method of *Matsuda et al.* [2014] to obtain wave number spectra of gravity waves, and we converted the wave number spectra to horizontal phase velocity spectra by using equation (1).

$$v_x = \frac{\omega k}{k^2 + l^2}\ ,\ v_y = \frac{\omega l}{k^2 + l^2} \tag{1}$$

Here v_x and v_y are the zonal and meridional components of the horizontal phase velocity, respectively, ω is the frequency, k is the zonal wave number, and l is the meridional wave number. For the conversion, we changed volume element by using the Jacobian determinant as shown by equations (2) and (3).

$$\mathrm{d}v_x \mathrm{d}v_y \mathrm{d}\omega = J \cdot \mathrm{d}k\mathrm{d}l\mathrm{d}\omega \tag{2}$$

$$J = \begin{vmatrix} \frac{\partial v_x}{\partial k} & \frac{\partial v_x}{\partial l} & \frac{\partial v_x}{\partial \omega} \\ \frac{\partial v_y}{\partial k} & \frac{\partial v_y}{\partial l} & \frac{\partial v_y}{\partial \omega} \\ 0 & 0 & 1 \end{vmatrix} \tag{3}$$

The spectra were obtained for horizontal wavelengths from 10 to 100 km for 557.7 nm and from 40 to 400 km for 630.0 nm. Finally, we integrated the horizontal phase velocity spectrum in all frequency ranges from 1/10.9 to 1/60.0 min (for the 5.0 min cadence) and from 1/11.0 to 1/60.5 min (for the 5.5 min cadence) for both 557.7 and 630.0 nm images.

4. Results and Discussion

In this section, we present the long-term variation of the horizontal phase velocity spectra and propagation direction for the mesospheric and thermospheric wave structures observed in airglow images, and we discuss the results. In the analysis, we defined the four seasons as follows: (1) spring: from 21 February to 19 April for 2 months, centering on the spring equinox; (2) summer: from 20 April to 20 August for 4 months, centering on the summer solstice; (3) fall: from 21 August to 19 October for 2 months, centering on the fall equinox; and (4) winter: from 20 October to 20 February for 4 months, centering on the winter solstice.

Summer and winter are longer than spring and fall because the dynamical variation of the middle atmosphere is divided into summer and winter types.

4.1. Results From 557.7 nm Airglow Images

Figure 1 shows the horizontal phase velocity spectra for the four seasons averaged over 16 years from 1999 to 2015 at Shigaraki, Japan. The power spectral density (PSD) indicates the power of the observed waves, corresponding to the square of the wave amplitude. These spectra are averages of all the 16 year spectra obtained in the analysis for each season. The power spectral density is calculated by summing all the power spectral density for 2–4 h time segments and dividing the summation by the number of time segments. The low-velocity region (0 to 20 m/s) shows high power spectral density because the white noise of airglow images contribute to enhance the power spectral density at the region of small wavelengths of images where the power spectral density from natural waves becomes relatively minor. The seasonal variations in the propagation direction of the gravity waves can be clearly identified in the higher-velocity region. In spring, the peak is northeastward and southwestward with a boundary of the power spectral intensity between yellow and green at ~70 m/s and ~40 m/s, respectively. In summer, the significant peak is north and northeastward with a boundary at ~70 m/s. In fall, the peak is northwestward with a boundary at ~60 m/s. In winter the peak is southwestward with a boundary at ~50 m/s. These seasonal variations of propagation direction are fairly consistent with those obtained by visual inspection in previous research (*Nakamura et al*. [1999] for Shigaraki and *Ejiri et al*. [2003] for Shigaraki and Rikubetsu).

Figure 2 shows the 16 year variation of the horizontal phase velocity spectrum and the propagation direction of gravity waves in the mesopause region obtained from the 3-D FFT analysis of 557.7 nm airglow images. These 16 year variations are obtained by integrating the horizontal velocity spectra for all phase velocities from 20 to 150 m/s. The spectra at 0–20 m/s were not used because of the white noise contamination of airglow images. Figure 2a shows the variations for all seasons, whereas Figures 2b–2e are for spring, summer, fall, and winter, respectively.

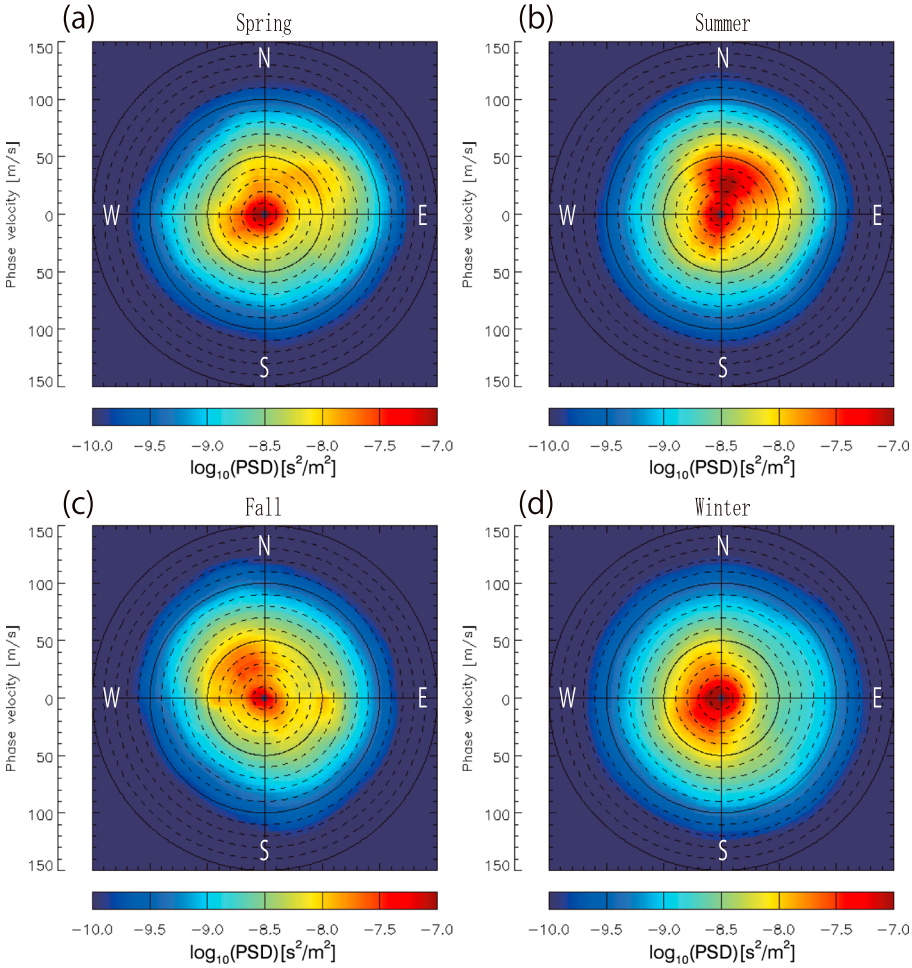

Figure 1. Sixteen year averages of horizontal phase velocity spectra in the mesopause region for (a) spring, (b) summer, (c) fall, and (d) winter. The tops of the spectra are pointing north, and the right sides are pointing east. Color bar indicates power spectral density (PSD) of the observed waves. The radius from the center indicates the phase velocity of gravity waves from 0 to 150 m/s.

In Figure 2a, the seasonal variation from the northeast, northwest, and southwest, which is repeated every year, is clearly visible. In Figures 2b–2e, more detailed variations in the propagation directions for the four seasons are seen. There is a clear difference in propagation direction between summer and winter. In summer, the propagation direction of gravity waves is continuously northeastward throughout the 16 years. However, in winter, the propagation direction of gravity waves is roughly southwestward but shows a much wider spread than in summer. In spring and fall, the propagation direction of gravity waves is either northeastward (summer type) or southwestward (winter type), and the predominant direction depends on the year. This is probably because the dynamics of the middle atmosphere are divided into summer and winter types, and spring and fall are transitional seasons.

In Figures 2b–2e, we also find several distinctive long-term variations in spectral intensity. In particular, the winter spectra shows clear variation of 5–7 years. Shorter-scale variations of 3–4 years can be also seen in summer.

4.2. Discussion of 557.7 nm Results

Next, we discuss the east-west anisotropy of the propagation direction during summer and winter, the north-south anisotropy of the propagation direction during summer and winter, and the characteristic yearly variations of spectral intensity in winter.

East-west anisotropy between summer and winter is probably caused by filtering of gravity waves by the mesospheric jet, which has a maximum wind velocity of about 70 m/s in the mesosphere [e.g., *Taylor et al.*, 1993].

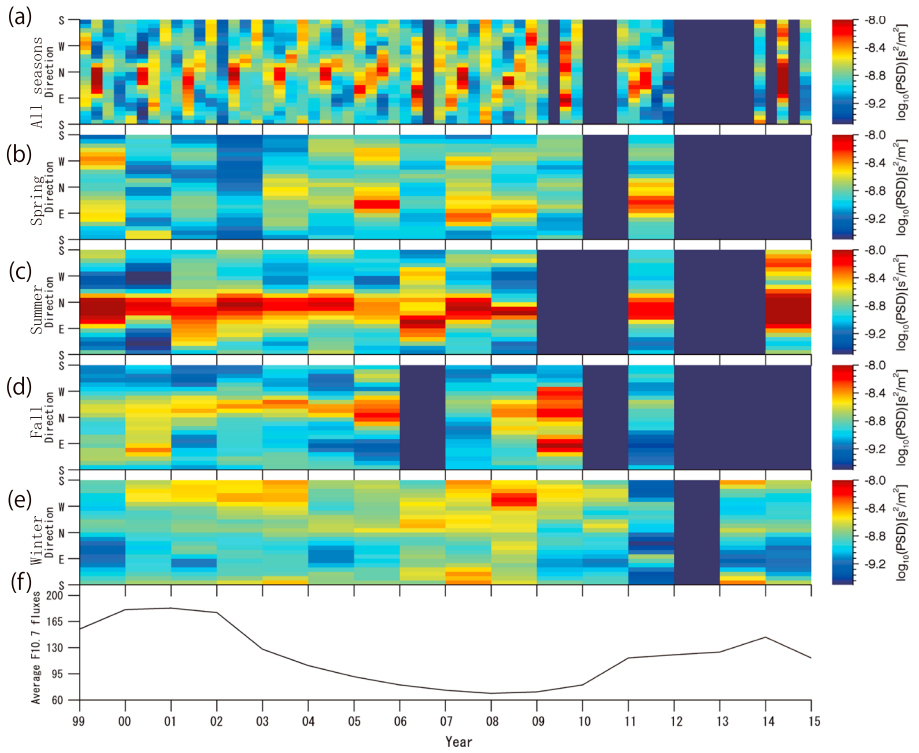

Figure 2. Sixteen year variation of horizontal phase velocity spectrum amplitude and propagation direction of gravity waves in the mesopause region obtained by 3-D FFT analysis of 557.7 nm airglow images. The horizontal axis shows the year from 1999 to 2015, and the vertical axis shows the azimuth angles. (a) All seasons, (b) spring, (c) summer, (d) fall, (e) winter, and (f) $F_{10.7}$ solar flux. Deep blue regions indicate years with no data.

The direction of the mesospheric jet is westward in summer and eastward in winter in both hemispheres. The dispersion relation of gravity waves is given as follows [*Hines*, 1960].

$$m^2 = \frac{N^2}{(c-u)^2} - k^2 - \frac{1}{4H^2} \tag{4}$$

Here m and k are vertical and horizontal wave numbers, respectively; c is horizontal phase velocity of gravity waves; u is background wind velocity; N is the Brant-Väisälä frequency; and H is scale height. According to equation (4), the waves that have a horizontal phase velocity (c) equal to the background wind velocity (u) cannot propagate further, because the vertical wave number (m) becomes infinity (critical level). Thus, if the propagation direction of the gravity waves is the same as that of the mesospheric jet and the horizontal phase velocity of the gravity wave is smaller than the mesospheric jet speed, the wave cannot propagate. This wind filtering effect causes the observed east-west anisotropy of the propagation direction in summer and winter [e.g., *Nakamura et al*., 1999; *Ejiri et al*., 2003].

This north-south anisotropy may be caused by the difference of the location of tropospheric gravity wave sources relative to Shigaraki. In this study, we investigated this possibility by using the tropospheric vertical flow velocity given by the ERA-Interim, which is one of the most reliable global atmospheric reanalysis data for the troposphere. We considered the source of the observed gravity waves as the convective activity in the troposphere, because the horizontal wavelengths of the observed waves are rather small (10–100 km). The gravity waves from the lower stratospheric jet stream would be in larger scale, considering the scale size of the jet stream. The orographic waves would be a stationary wave which does not have horizontal phase velocity. For ERA-Interim, the time resolution is 6 h and both longitudinal and latitudinal spatial resolution are 0.75°. We used the pressure vertical velocities at 400 hPa on the pressure coordinates, which corresponds to an altitude of about 7 km in the middle latitudes. This height was chosen because it is the middle part of the troposphere. Thus, the upward flow in this height indicates existence of rather strong convection activity.

Figures 3a and 3b show the pressure vertical velocity (negative: upward) averaged over summer and winter at 400 hPa on the pressure coordinates (~7 km in altitudes) from the European Centre for Medium-Range

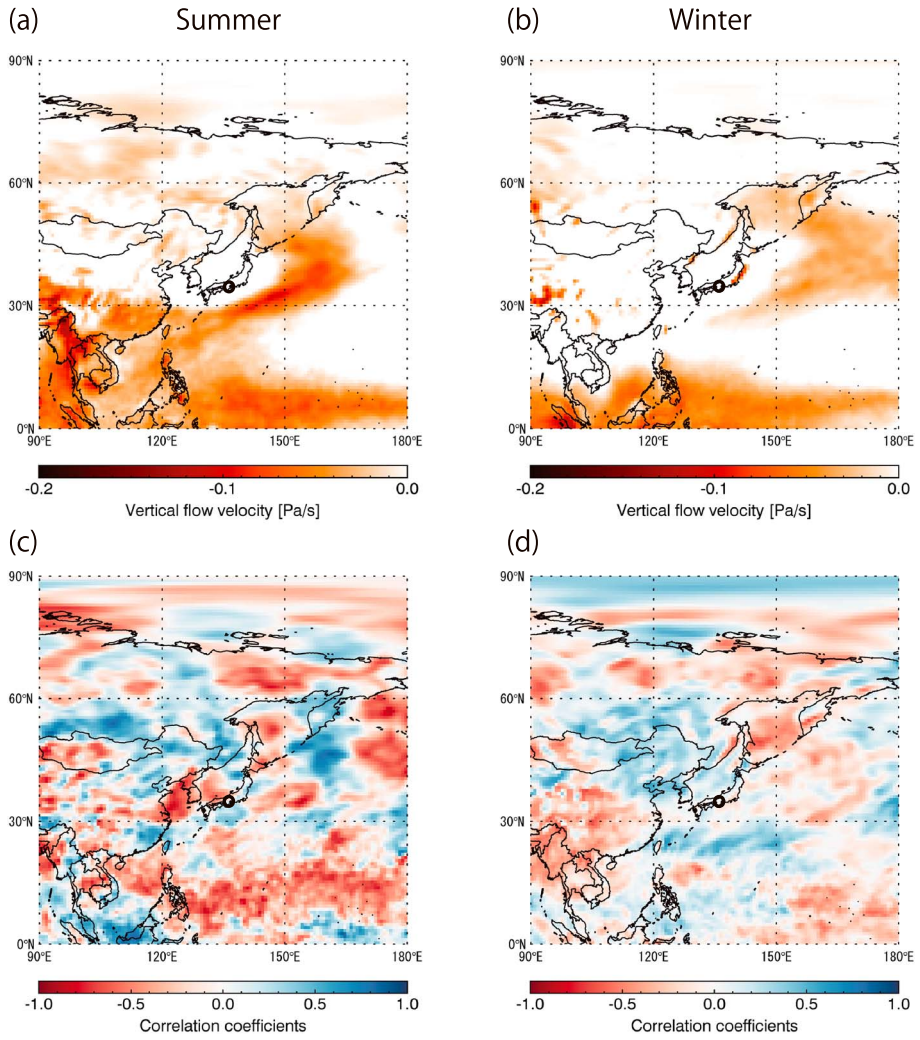

Figure 3. (a) Summer and (b) winter averages of the pressure vertical velocity (negative: upward) at 400 hPa at the pressure coordinates calculated by ERA-Interim for the dates when the 557.7 nm airglow images are available. (c) Summer and (d) winter correlation coefficients between the yearly power spectrum amplitude of the horizontal phase velocity and yearly vertical velocity in Figures 3a and 3b, respectively. Red regions (negative correlation coefficients) indicate a positive correlation between the upward flow and high power spectral density because negative vertical velocity indicates upward flow. The small black circle indicates the Shigaraki airglow imager station.

Weather Forecasts (ECMWF) interim reanalysis (ERA-Interim) [*Dee et al.*, 2011]. The small black circle indicates the airglow imager station at Shigaraki. We averaged the data for the dates when the 557.7 nm airglow images are available. This data set corresponds to particular weather conditions when the night sky was clear over Shigaraki. In summer, there is a region of strong upward velocities from the south to the east of Japan due to the Baiu rain band on a line approximately from (20°N, 120°E) to (40°N, 170°E) and at latitudes from 0°N to 10°N near the equator. If gravity waves were generated in these regions, the propagation direction at Shigaraki would be northward and westward, while the westward propagating waves will be filtered out by the mesospheric jet in summer. In winter, there is a region of strong vertical velocities in the northeast of Japan due to wintry extratropical cyclones. If gravity waves were generated in this region, the propagation direction would be southwestward. These results indicate that the observed north-south anisotropy of gravity waves in the 557.7 nm airglow images could be caused by the difference in the location of gravity wave sources in the troposphere.

The distance between these possible source regions of gravity waves and Shigaraki could be more than 1000 km. This distance may be too far for the horizontal propagation of small-scale gravity waves from the troposphere to the mesopause region [e.g., *Alexander*, 1996; *Horinouchi et al.*, 2002]. According to

Suzuki et al. [2013] and *Parihar and Taori* [2015], atmospheric gravity waves ducting in the mesopause region propagate over long distances (1200–2000 km). *Walterscheid et al.* [2001] reported that ducting waves may propagate over more than 2000 km distances. A mesospheric duct is necessary for propagation of small-scale gravity waves over such long distances from possible source regions in the troposphere to the mesopouse region over Shigaraki.

Next, we discuss the 5–7 year variation of the spectral intensity of the horizontal phase velocity in winter. We investigated the correlation between the yearly variations of the spectral intensity and the following four parameters: tropospheric vertical flow velocity obtained by the ERA-Interim reanalysis data; the NINO3 index [*Torrence and Compo*, 1998], which is a proxy for the El Niño–Southern Oscillation and has a 2–7 year periodicity; the AO index [*Thompson and Wallace*, 1998], which is a proxy for the Arctic Oscillation and has a 6–15 year periodicity; and the $F_{10.7}$ solar flux [*Tapping*, 1987], which is a proxy for solar activity and has an 11 year periodicity. El Niño–Southern Oscillation, Arctic Oscillation, and solar activity affect climate at middle latitudes through causing long-term variations of temperature, atmospheric pressure, and wind field [*Sakai and Kawamura*, 2009; *Park et al.*, 2011]. These long-term variations may cause the variation of the spectral intensity of the horizontal phase velocity in winter.

Figures 3c and 3d show the correlation coefficient between the yearly averages of the spectral intensities of the horizontal phase velocity and the yearly averages of the tropospheric vertical flow velocities. This analysis is made to identify possible connection between the yearly variations of gravity wave power observed in the airglow images and the yearly variations of the possible source convection activities in the troposphere. In summer in Figure 3a, there are strong upward flow regions in the Baiu front and at latitudes from 0°N to 10°N near the equator, as noted before. In Figure 3c, several high correlation regions (red) are also seen in these strong upward flow regions. In winter, the region of strong vertical velocities in the northeast of Japan also corresponds to the high correlation region in Figure 3d. These positive correlations between the spectral intensity of the gravity waves in the 557.7 nm airglow images and the tropospheric vertical flow velocity suggest that the yearly variation of gravity wave power in the airglow images can be caused by the variations of the tropospheric source activities, though there may be some other causes for the yearly variation of gravity wave power in airglow images, such as yearly variations of mesospheric wind velocities.

On the other hand, the correlation coefficients of the spectral intensity of gravity waves in winter with the NINO3 index and with the AO index are 0.034 and −0.151, respectively, indicating no correlation with these parameters. The correlation coefficients with the $F_{10.7}$ solar flux is 0.032, indicating no correlation between the solar activity and the gravity wave intensity in the mesopause region. We used airglow images for only clear-sky nights, which may affect these low correlation coefficients.

4.3. Results From 630.0 nm Airglow Images

Figure 4 shows the horizontal phase velocity spectra obtained from 630.0 nm airglow images in four seasons averaged over 16 years from 1999 to 2015 at Shigaraki, Japan. In these spectra, the major propagation direction of the waves is always southwestward, consistent with many previous studies by visual inspection, and the waves probably correspond to nighttime MSTIDs [e.g., *Saito et al*., 1998; *Garcia et al*., 2000; *Shiokawa et al.*, 2003b; *Otsuka et al*., 2004]. A minor northeastward propagating component is also seen in these four panels. This northeastward propagating component is newly identified by the 3-D FFT method. In spring and fall, the peak is southwestward with a power spectral intensity boundary between yellow and green at ∼110 m/s. In summer, the boundary is at ∼180 m/s, and in winter, the boundary is at ∼140 m/s. In summer, the highest power spectral density and horizontal phase speed of the wave are observed. The minor northeastward propagating component is also the largest power spectral density during summer.

Figure 5 shows the 16 year variation of the horizontal phase velocity spectra and propagation direction of waves in the thermosphere obtained from the 3-D FFT analysis of 630.0 nm airglow images. These 16 year variations are obtained by integrating the horizontal velocity spectra for all phase velocities from 40 to 300 m/s. The spectra at 0–40 m/s were not used because of the white noise contamination of airglow images. Figure 5a shows the variations for all seasons, whereas Figures 5b–5e show those for spring, summer, fall, and winter, respectively.

In Figure 5a, the propagation direction of waves is always southwestward with a minor northeastward propagating component throughout the 16 years. The power spectral intensities show long-term variations, increasing between 2001 and 2007 and then decreasing after ∼2009. Figures 5b–5e show the variations

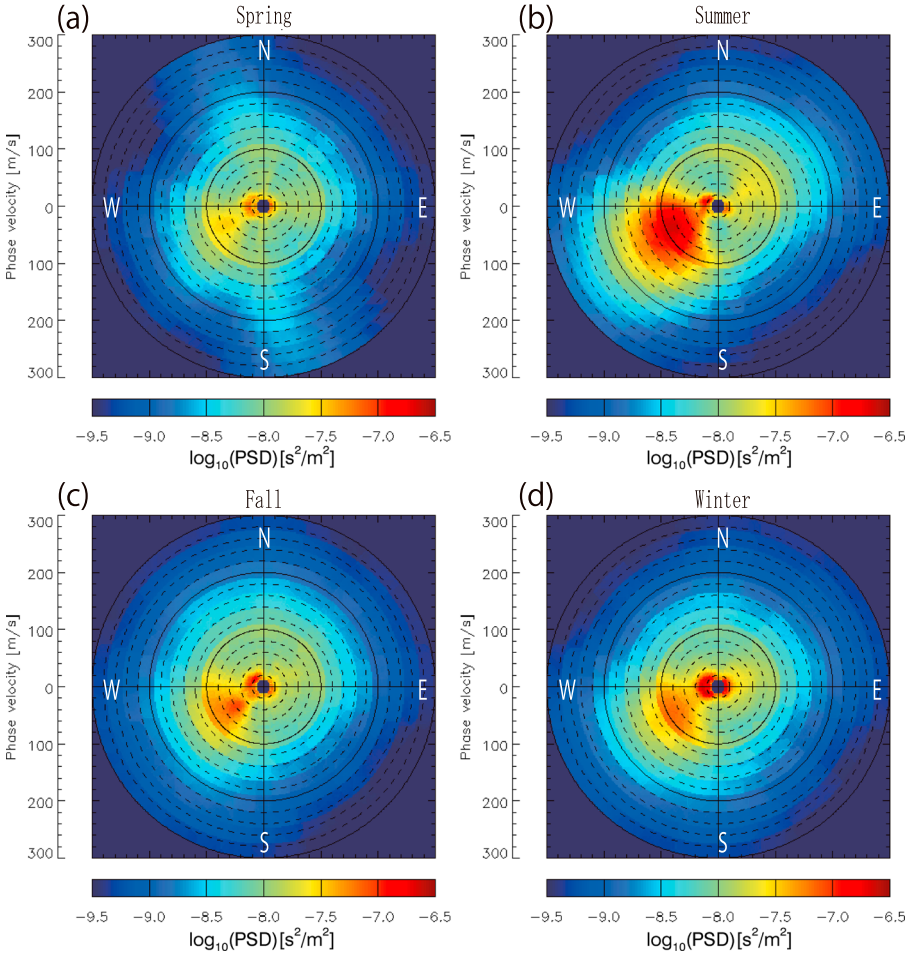

Figure 4. Sixteen year averages of horizontal phase velocity spectra in the thermosphere obtained from the 630.0 nm airglow images for (a) spring, (b) summer, (c) fall, and (d) winter. The tops of the spectra are pointing north, and the right sides are pointing east. The radius from the center indicates the phase velocity of MSTIDs from 0 to 300 m/s.

during the four seasons. All seasons have the major southwestward component and the minor northeastward component. The variations in the power spectral intensities also show a similar trend, in which the intensity increases between ~2001 and ~2007 and then decreases after ~2009. Figure 5f shows the yearly average of the $F_{10.7}$ solar flux. A clear negative correlation is seen between the variation in the power spectral intensities and the $F_{10.7}$ solar flux, with correlation coefficients of −0.894 and −0.663 for summer and winter, respectively.

4.4. Discussion of 630.0 nm Results

According to *Hunsucker* [1982], the wavelength of large-scale TIDs (LSTIDs) is over 1000 km, while the wavelength of MSTIDs is several hundred kilometers. The term small-scale TIDs has not been used after *Hunsucker* [1982]. The scale sizes of waves we studied using the 630.0 nm airglow images are 40–400 km. Thus, we consider the waves we analyzed in this paper using the 630.0 nm airglow images as MSTIDs.

Figure 5 shows a rather clear negative correlation between the variation in the power spectral intensities and the $F_{10.7}$ solar flux. Some papers reported the negative relationship in occurrence of nighttime MSTIDs with solar activity [*Duly et al.*, 2013; *Narayanan et al.*, 2014]. To explain this negative correlation, we consider the growth rate of the Perkins instability, which plays an important role in generating the nighttime MSTIDs at middle latitudes [*Perkins*, 1973; *Yokoyama et al.*, 2009]. Equation (5) shows the linear growth rate of the Perkins instability.

$$\gamma = \frac{g \sin^2 I}{\nu_{in} H_n} \tag{5}$$

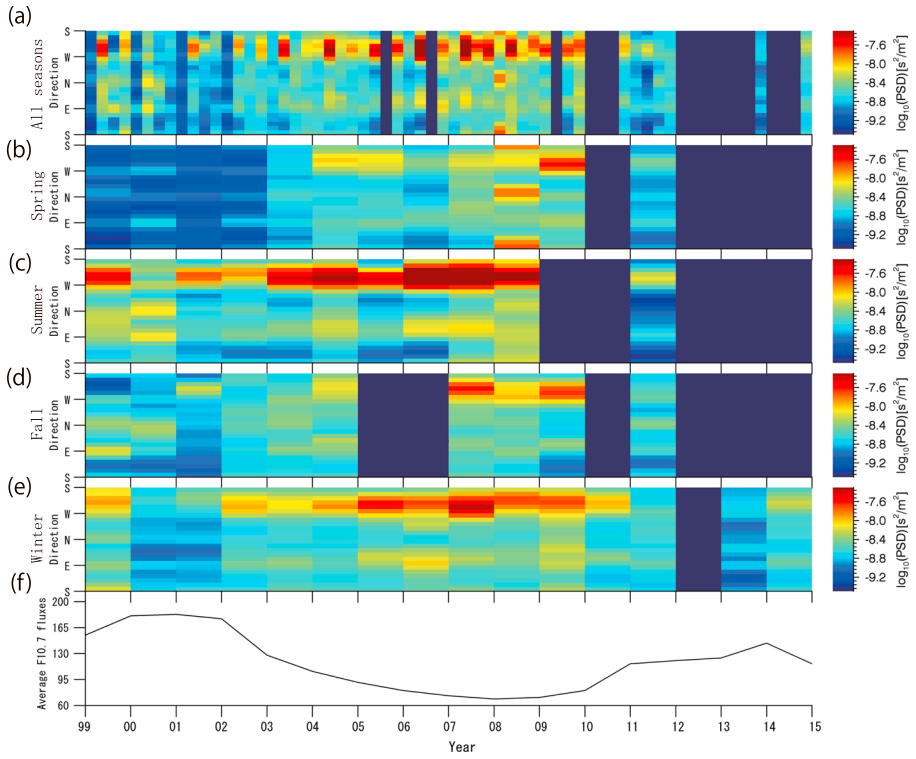

Figure 5. Sixteen year variation of horizontal phase velocity spectra and propagation direction of waves in the thermosphere obtained from 3-D FFT analysis of 630.0 nm airglow images. The horizontal axis shows the year from 1999 to 2015, and the vertical axis shows the azimuth angles. (a) All seasons, (b) spring, (c) summer, (d) fall, (e) winter, and (f) $F_{10.7}$ solar flux. Deep blue areas indicate years with no data.

Here I is the magnetic inclination, g is the acceleration due to gravity, ν_{in} is the ion-neutral collision frequency, and H_n is the scale height. ν_{in} and H_n are affected by solar activity. The typical values of ν_{in} and H_n in the lower thermosphere are 6 s^{-1} and 45 km, respectively. When solar activity is small, ν_{in} and H_n are small. Then, the linear growth rate of the Perkins instability, γ, will be large. This could cause the clear negative correlation between the power spectral intensities and $F_{10.7}$ solar flux in Figure 5.

Otsuka et al. [2007] and *Yokoyama et al.* [2009] pointed out that the sporadic *E* layer instability plays a major role in generating the nighttime MSTIDs, and the Perkins instability helps to amplify its perturbation. In this study, the clear negative correlation implies that the Perkins instability plays also an important role in generating the nighttime MSTIDs at middle latitudes, in addition to the *E-F* coupling process in the nighttime ionosphere at middle latitudes.

Gravity waves propagating from the lower atmosphere can initiate the ionospheric instabilities that may result in the MSTIDs. *Vadas et al.* [2014] suggested that gravity wave penetration is less important and secondary wave generation is more important during the solar quiet time. This is because during solar minimum, the background density decreases more rapidly with increasing altitudes, causing the kinematic viscosity to increase more rapidly with altitudes. Kinematic viscosity makes gravity waves fragile, allowing secondary waves to be generated. The secondary waves propagate to the thermosphere and may trigger the MSTIDs. This scenario may also explain the negative correlation between MSTIDs activity in the thermosphere and the solar activity, which is consistent with our long-term analysis.

Many previous studies of 630 nm airglow images by visual inspection reported that nighttime MSTIDs propagate mainly southwestward. *Yokoyama et al.* [2009] suggested that the southward neutral wind in the sporadic *E* layer arising from atmospheric tides produces MSTIDs propagating southward. However, Figure 5 shows a minor northeastward component of MSTIDs, which is newly identified by this 3-D FFT method. If the southward neutral wind in the sporadic *E* layer always makes MSTIDs propagate southward, we could not explain the northeastward propagating component. *Shiokawa et al.* [2008] reported an event observed at Paratunka, Kamchatka (north of Japan), during which the MSTIDs propagated first southwestward, and

then northeastward. If the variation of the neutral wind in the sporadic *E* layer is caused by atmospheric tides, it may exhibit latitudinal dependence on their characteristics. Thus, more studies of this sort of 3-D FFT analysis for stations at different latitudes may contribute to understanding the mechanisms that determine the propagation direction of MSTIDs.

5. Summary and Concluding Remarks

In this study, we used the 3-D FFT method developed by *Matsuda et al.* [2014] to analyze the horizontal phase velocity spectra of gravity waves and MSTIDs observed in 557.7 nm (altitude of 90–100 km in the mesopause region) and 630.0 nm (altitude of 200–300 km in the thermosphere and ionosphere) airglow images obtained at Shigaraki MU Observatory (34.8°N, 136.1°E) over ~16 years, from 16 March 1999 to 20 February 2015. We found several interesting features of the long-term variation of these horizontal phase velocity spectra. Our results can be summarized as follows.

1. In the mesopause region in the 557.7 nm airglow images, there are clear seasonal variations in the propagation direction of gravity waves. In spring, the peak is northeastward and southwestward with a boundary of the power spectral intensity between yellow and green at ~70 m/s and ~40 m/s respectively. In summer, the significant peak is north and northeastward with a boundary at ~70 m/s. In fall, the peak is northwestward with a boundary at ~60 m/s. In winter the peak is southwestward with a boundary at ~50 m/s. This seasonal variation of the propagation direction is repeated every year.
2. The propagation directions between summer (northeastward) and winter (southwestward) are anisotropic in the mesopause region. The east-west anisotropy is probably caused by the filtering of gravity waves by the mesospheric jet. The north-south anisotropy is possibly caused by the difference in the location of gravity wave sources. By comparing the tropospheric reanalysis data (vertical velocity at 400 hPa) of ERA-Interim, we identified the gravity wave source in the troposphere as the Baiu front and the tropical convection activities in the south of Japan in summer and the wintry low pressure in the northeast of Japan in winter.
3. There are several distinctive long-term variations in the spectral intensities of the gravity waves in the mesopause region. In particular, the winter spectra shows clear variation of 5–7 years. There are positive correlations between the yearly power spectral intensity of gravity waves and the yearly upward velocity at 400 hPa at several regions in the south of Japan in summer and in northeastern Japan in winter. However, there is no clear correlation between the spectral variation and the NINO3 and AO indices and $F_{10.7}$ solar flux in winter.
4. In the thermosphere and ionosphere in 630.0 nm airglow images, the propagation direction of waves is always southwestward throughout the 16 years. These waves probably correspond to the nighttime MSTIDs reported in previous work. In spring, summer, fall, and winter, the peak velocities of the spectra are less than ~110, ~180, ~110, and ~140 m/s, respectively. In summer, the highest power spectral density and horizontal phase velocity of the waves are observed. We also found a clear minor peak for the northeastward propagating component of MSTIDs.
5. The power spectral intensities of the MSTIDs for four seasons show long-term variation, increasing between 2001 and 2007, and then decreasing until 2011. There is a clear negative correlation between these variations of the power spectral intensities and $F_{10.7}$ solar flux. This anticorrelation of MSTIDs with solar activity is consistent with the linear growth rate of the Perkins instability and the secondary wave generation of gravity waves in the thermosphere.

Acknowledgments
We thank Y. Katoh, M. Satoh, T. Katoh, Y. Hamaguchi, Y. Yamamoto, and T. Adachi of the Solar-Terrestrial Environment Laboratory/Institute for Space-Earth Environmental Research (ISEE), Nagoya University, for their helpful support with the airglow imaging observations. The MU radar at Shigaraki belongs to and is operated by the Research Institute for Sustainable Humanosphere, Kyoto University. The all-sky airglow images used in the present study are available at ISEE, Nagoya University. ERA-Interim data used in Figure 3 are available at the European Centre for Medium-Range Weather Forecasts (ECMWF). The NINO3 index, AO index, and $F_{10.7}$ index used in this paper are available at http://www.data.jma.go.jp/gmd/cpd/db/elnino/index/soi.html, http://www.cpc.ncep.noaa.gov/products/precip/CWlink/daily_ao_index/ao.shtml, and http://omniweb.gsfc.nasa.gov/form/dx1.html, respectively.
This research is supported by the JSPS Core-to-Core Program, B. Asia-Africa Science Platforms, and JSPS KAKENHI grants (JP 15H05815 and JP 16H06286).

References

Alexander, M. J. (1996), A simulated spectrum of convectively generated gravity waves: Propagation from the tropopause to the mesopause and effects on the middle atmosphere, *J. Geophys. Res.*, *101*(D1), 1571–1588, doi:10.1029/95JD02046.

Dee, D. P., et al. (2011), The ERA-Interim reanalysis: Configuration and performance of the data assimilation system, *Q. J. R. Meteorol. Soc.*, *137*, 553–597, doi:10.1002/Qj.828.

Duly, T. M., N. P. Chapagain, and J. J. Makela (2013), Climatology of nighttime medium-scale traveling ionospheric disturbances (MSTIDs) in the Central Pacific and South American sectors, *Ann. Geophys.*, *31*, 2229–2237, doi:10.5194/angeo-31-2229-2013.

Ejiri, M. K., K. Shiokawa, T. Ogawa, K. Igarashi, T. Nakamura, and T. Tsuda (2003), Statistical study of short-period gravity waves in OH and OI nightglow images at two separated sites, *J. Geophys. Res.*, *108*(D21), 4679, doi:10.1029/2002JD002795.

Garcia, F., M. C. Kelley, and J. J. Makela (2000), Airglow observations of mesoscale low-velocity traveling ionospheric disturbances at midlatitudes, *J. Geophys. Res.*, *105*(A8), 18,407–18,415, doi:10.1029/1999JA000305.

Hecht, J. H., R. L. Walterscheid, and M. N. Ross (1994), First measurements of the two-dimensional horizontal wave number spectrum from CCD images of the nightglow, *J. Geophys. Res.*, *99*(A6), 11,449–11,460, doi:10.1029/94JA00584.

Hines, C. O. (1960), Internal atmospheric gravity waves at ionospheric heights, *Can. J. Phys.*, *38*, 1441–1481.

Horinouchi, T., T. Nakamura, and J.-i. Kosaka (2002), Convectively generated mesoscale gravity waves simulated throughout the middle atmosphere, *Geophys. Res. Lett.*, *29*(21), 2007, doi:10.1029/2002GL016069.
Hunsucker, R. D. (1982), Atmospheric gravity waves generated in the high-latitude ionosphere: A review, *Rev. Geophys.*, *20*, 293–315.
Kubota, M., K. Shiokawa, M. K. Ejiri, Y. Otsuka, T. Ogawa, T. Sakanoi, H. Fukunishi, M. Yamamoto, S. Fukao, and A. Saito (2000), Traveling ionospheric disturbances observed in the OI 630-nm nightglow images over Japan by using a multipoint imager network during the FRONT campaign, *Geophys. Res. Lett.*, *27*(24), 4037–4040, doi:10.1029/2000GL011858.
Makela, J. J., and M. C. Kelley (2003), Using the 630.0-nm nightglow emission as a surrogate for the ionospheric Pedersen conductivity, *J. Geophys. Res.*, *108*(A6), 1253, doi:10.1029/2003JA009894.
Martinis, C., J. Baumgardner, J. Wroten, and M. Mendillo (2010), Seasonal dependence of MSTIDs obtained from 630.0 nm airglow imaging at Arecibo, *Geophys. Res. Lett.*, *37*, L11103, doi:10.1029/2010GL043569.
Matsuda, T. S., T. Nakamura, M. K. Ejiri, M. Tsutsumi, and K. Shiokawa (2014), New statistical analysis of the horizontal phase velocity distribution of gravity waves observed by airglow imaging, *J. Geophys. Res. Atmos.*, *119*, 9707–9718, doi:10.1002/2014JD021543.
Nakamura, T., A. Higashikawa, T. Tsuda, and Y. Matsushita (1999), Seasonal variations of gravity wave structures in OH airglow with a CCD imager at Shigaraki, *Earth Planets Space*, *51*, 897–906.
Narayanan, V. L., K. Shiokawa, Y. Otsuka, and S. Saito (2014), Airglow observations of nighttime medium-scale traveling ionospheric disturbances from Yonaguni: Statistical characteristics and low-latitude limit, *J. Geophys. Res. Space Physics*, *119*, 9268–9282, doi:10.1002/2014JA020368.
Otsuka, Y., K. Shiokawa, T. Ogawa, and P. Wilkinson (2004), Geomagnetic conjugate observations of medium-scale traveling ionospheric disturbances at midlatitude using all-sky airglow imagers, *Geophys. Res. Lett.*, *31*, L15803, doi:10.1029/2004GL020262.
Otsuka, Y., F. Onoma, K. Shiokawa, T. Ogawa, M. Yamamoto, and S. Fukao (2007), Simultaneous observations of nighttime medium-scale traveling ionospheric disturbances and *E* region field-aligned irregularities at midlatitude, *J. Geophys. Res.*, *112*, A06317, doi:10.1029/2005JA011548.
Parihar, N., and A. Taori (2015), An investigation of long-distance propagation of gravity waves under CAWSES India Phase II Programme, *Ann. Geophys.*, *33*, 547–560, doi:10.5194/angeo-33-547-2015.
Park, T. W., C. H. Ho, and S. Yang (2011), Relationship between the Arctic oscillation and cold surges over East Asia, *J. Clim.*, *24*, 68–83.
Perkins, F. (1973), Spread F and ionospheric currents, *J. Geophys. Res.*, *78*, 218–226.
Saito, A., S. Fukao, and S. Miyazaki (1998), High resolution mapping of TEC perturbations with the GSI GPS network over Japan, *Geophys. Res. Lett.*, *25*, 3079–3082.
Saito, A., et al. (2001), Traveling ionospheric disturbances detected in the FRONT campaign, *Geophys. Res. Lett.*, *28*(4), 689–692, doi:10.1029/2000GL011884.
Sakai, K., and R. Kawamura (2009), Remote response of the East Asian winter monsoon to tropical forcing related to El Niño–Southern Oscillation, *J. Geophys. Res.*, *114*, D06105, doi:10.1029/2008JD010824.
Shefov, N. N., A. I. Semenov, and O. T. Yurchenko (2007), Empirical model of the OI 630 nm emission variations. 3. Emitting layer height, *Geomagn. Aeron.*, *47*, 750–755, doi:10.1134/S0016793207060072.
Shiokawa, K., Y. Katoh, M. Satoh, M. Ejiri, T. Ogawa, T. Nakamura, T. Tsuda, and R. Wiens (1999), Development of Optical Mesosphere Thermosphere Imagers (OMTI), *Earth Planets Space*, *51*, 887–896.
Shiokawa, K., C. Ihara, Y. Otsuka, and T. Ogawa (2003a), Statistical study of nighttime medium-scale traveling ionospheric disturbances using midlatitude airglow imagers, *J. Geophys. Res.*, *108*(A1), 1052, doi:10.1029/2002JA009491.
Shiokawa, K., Y. Otsuka, C. Ihara, T. Ogawa, and F. J. Rich (2003b), Ground and satellite observations of nighttime medium-scale traveling ionospheric disturbance at midlatitude, *J. Geophys. Res.*, *108*(A4), 1145, doi:10.1029/2002JA009639.
Shiokawa, K., Y. Otsuka, N. Nishitani, T. Ogawa, T. Tsugawa, T. Maruyama, S. E. Smirnov, V. V. Bychkov, and B. M. Shevtsov (2008), Northeastward motion of nighttime medium-scale traveling ionospheric disturbances at middle latitudes observed by an airglow imager, *J. Geophys. Res.*, *113*, A12312, doi:10.1029/2008JA013417.
Shiokawa, K., Y. Otsuka, and T. Ogawa (2009), Propagation characteristics of nighttime mesospheric and thermospheric waves observed by optical mesosphere thermosphere imagers at middle and low latitudes, *Earth Planets Space*, *61*, 479–491.
Suzuki, S., K. Shiokawa, Y. Otsuka, S. Kawamura, and Y. Murayama (2013), Evidence of gravity wave ducting in the mesopause region from airglow network observations, *Geophys. Res. Lett.*, *40*, 601–605, doi:10.1029/2012GL054605.
Swenson, G. R., R. Haque, W. Yang, and C. S. Gardner (1999), Momentum and energy fluxes of monochromatic gravity waves observed by an OH imager at Starfire Optical Range, New Mexico, *J. Geophys. Res.*, *104*(D6), 6067–6080, doi:10.1029/1998JD200080.
Tapping, K. F. (1987), Recent solar radio astronomy at centimeter wavelengths: The temporal variability of the 10.7-cm flux, *J. Geophys. Res.*, *92*(D1), 829-838, doi:10.1029/JD092id01p00829.
Taylor, M. J., E. H. Ryan, T. F. Tuan, and R. Edwards (1993), Evidence of preferential directions for gravity wave propagation due to wind filtering in the middle atmosphere, *J. Geophys. Res.*, *98*(A4), 6047–6057, doi:10.1029/92JA02604.
Taylor, M. J., J.-M. Jahn, S. Fukao, and A. Saito (1998), Possible evidence of gravity wave coupling into the mid-latitude *F* region ionosphere during the SEEK Campaign, *Geophys. Res. Lett.*, *25*(11), 1801–1804, doi:10.1029/97GL03448.
Thompson, D. W. J., and J. M. Wallace (1998), The Arctic Oscillation signature in the wintertime geopotential height and temperature fields, *Geophys. Res. Lett.*, *25*, 1297–1300, doi:10.1029/98GL00950.
Torrence, C., and G. Compo (1998), A practical guide to wavelet analysis, *Bull. Am. Meteorol. Soc.*, *79*, 61–78.
Vadas, S. L., H.-L. Liu, and R. S. Lieberman (2014), Numerical modeling of the global changes to the thermosphere and ionosphere from the dissipation of gravity waves from deep convection, *J. Geophys. Res. Space Physics*, *119*, 7762–7793, doi:10.1002/2014JA020280.
Walterscheid, R. L., G. Schubert, and D. G. Brinkman (2001), Small-scale gravity waves in the upper mesosphere and lower thermosphere generated by deep tropical convection, *J. Geophys. Res.*, *106*(D23), 31,825–31,832, doi:10.1029/2000JD000131.
Yokoyama, T., D. L. Hysell, Y. Otsuka, and M. Yamamoto (2009), Three-dimensional simulation of the coupled Perkins and E_S-layer instabilities in the nighttime midlatitude ionosphere, *J. Geophys. Res.*, *114*, A03308, doi:10.1029/2008JA013789.
Yue, J., T. Nakamura, C.-Y. She, M. Weber, W. Lyons, and T. Li (2010), Seasonal and local time variability of ripples from airglow imager observations in US and Japan, *Ann. Geophys.*, *28*, 1401–1408, doi:10.5194/angeo-28-1401-2010.